Apicidin Attenuates MRSA Virulence through Quorum-Sensing Inhibition and Enhanced Host Defense

By: Corey P. Parlet, Jeffrey S. Kavanaugh, Heidi A. Crosby, Huzefa A. Raja, Tamam El-Elimat, Daniel A. Todd, Cedric J. Pearce, Nadja B. Cech, Nicholas H. Oberlies, and Alexander R. Horswill

Parlet, C. P., Kavanaugh, J. S., Crosby, H. A., Raja, H. A., El-Elimat, T., Todd, D. A., Pearce, C. J., Cech, N. B., Oberlies, N. H., & Horswill, A. R. (2019). Apicidin Attenuates MRSA Virulence through Quorum-Sensing Inhibition and Enhanced Host Defense. *Cell Reports, 27*(1), 187-198. https://doi.org/10.1016/j.celrep.2019.03.018

Abstract:

Recurrent epidemics of drug-resistant *Staphylococcus aureus* illustrate the rapid lapse of antibiotic efficacy following clinical implementation. Over the last decade, community-associated methicillin-resistant *S. aureus* (MRSA) has emerged as a dominant cause of infections, and this problem is amplified by the hyper-virulent nature of these isolates. Herein, we report the discovery of a fungal metabolite, apicidin, as an innovative means to counter both resistance and virulence. Owing to its breadth and specificity as a quorum-sensing inhibitor, apicidin antagonizes all MRSA *agr* systems in a non-biocidal manner. In skin challenge experiments, the apicidin-mediated abatement of MRSA pathogenesis corresponds with quorum-sensing inhibition at *in vivo* sites of infection. Additionally, we show that apicidin attenuates MRSA-induced disease by potentiating innate effector responses, particularly through enhanced neutrophil accumulation and function at cutaneous challenge sites. Together, these results indicate that apicidin treatment represents a strategy to limit MRSA virulence and promote host defense.

Keywords: *Staphylococcus aureus* | MRSA | quorum sensing | *agr* | apicidin | natural product | pathogenesis | skin infection

Article:

***Note: Full text of article below**

Article

Cell Reports

Apicidin Attenuates MRSA Virulence through Quorum-Sensing Inhibition and Enhanced Host Defense

Graphical Abstract

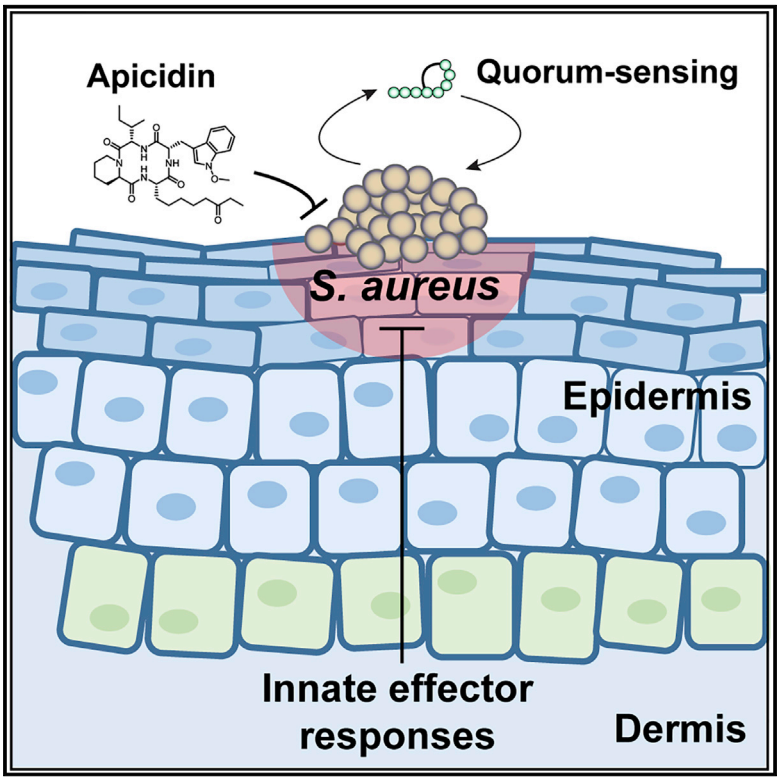

Authors

Corey P. Parlet, Jeffrey S. Kavanaugh, Heidi A. Crosby, ..., Nadja B. Cech, Nicholas H. Oberlies, Alexander R. Horswill

Correspondence

alexander.horswill@ucdenver.edu

In Brief

Parlet et al. identified the apicidin family of fungal-derived compounds as potent inhibitors of *Staphylococcus aureus agr* quorum sensing. In a mouse model of skin infection, apicidin prevented *agr* activation and MRSA-induced dermonecrosis. Apicidin treatment also induced neutrophil accumulation and function at MRSA challenge sites, aiding host defense to infection.

Highlights

- Apicidin is a fungal-derived *agr* quorum-sensing inhibitor of *S. aureus*
- Apicidin prevents *agr* activation and MRSA-induced dermonecrosis during skin infection
- Treatment with apicidin enhances host defense to MRSA by augmenting innate immunity

Parlet et al., 2019, Cell Reports *27*, 187–198
April 2, 2019
https://doi.org/10.1016/j.celrep.2019.03.018

CellPress

Cell Reports
Article

Apicidin Attenuates MRSA Virulence through Quorum-Sensing Inhibition and Enhanced Host Defense

Corey P. Parlet,[1] Jeffrey S. Kavanaugh,[2] Heidi A. Crosby,[2] Huzefa A. Raja,[3] Tamam El-Elimat,[3] Daniel A. Todd,[3] Cedric J. Pearce,[4] Nadja B. Cech,[3] Nicholas H. Oberlies,[3] and Alexander R. Horswill[2,5,6,*]
[1]Roy J. and Lucille A. Carver College of Medicine, Department of Microbiology, University of Iowa, Iowa City, IA, USA
[2]Department of Immunology and Microbiology, University of Colorado School of Medicine, Aurora, CO, USA
[3]Department of Chemistry and Biochemistry, University of North Carolina at Greensboro, Greensboro, NC, USA
[4]Mycosynthetix, Inc., Hillsborough, NC, USA
[5]Department of Veterans Affairs, Eastern Colorado Healthcare System, Aurora, CO, USA
[6]Lead Contact
*Correspondence: alexander.horswill@ucdenver.edu
https://doi.org/10.1016/j.celrep.2019.03.018

SUMMARY

Recurrent epidemics of drug-resistant *Staphylococcus aureus* illustrate the rapid lapse of antibiotic efficacy following clinical implementation. Over the last decade, community-associated methicillin-resistant *S. aureus* (MRSA) has emerged as a dominant cause of infections, and this problem is amplified by the hyper-virulent nature of these isolates. Herein, we report the discovery of a fungal metabolite, apicidin, as an innovative means to counter both resistance and virulence. Owing to its breadth and specificity as a quorum-sensing inhibitor, apicidin antagonizes all MRSA *agr* systems in a non-biocidal manner. In skin challenge experiments, the apicidin-mediated abatement of MRSA pathogenesis corresponds with quorum-sensing inhibition at *in vivo* sites of infection. Additionally, we show that apicidin attenuates MRSA-induced disease by potentiating innate effector responses, particularly through enhanced neutrophil accumulation and function at cutaneous challenge sites. Together, these results indicate that apicidin treatment represents a strategy to limit MRSA virulence and promote host defense.

INTRODUCTION

Antibiotic-resistant pathogens threaten human health and economic stability on a global scale (Laxminarayan et al., 2013; Medina and Pieper, 2016). A common theme among recent reports from the World Health Organization, US Centers for Disease Control and Prevention, the European Centre for Disease Prevention and Control, the NIH, and the World Economic Forum is that the post-antibiotic era looms ever closer as the loss of efficacy among available antibiotics is far outpacing the generation of effective replacements (CDC, 2013; NIAID, 2014; O'Neill, 2016; Spellberg et al., 2016). Failure to reverse these trends could lead to an exhaustion of protective interventions against top pathogens. According to the Review on Antimicrobial Resistance, infectious diseases are poised to claim 10 million lives per year and account for 100 trillion dollars of lost economic output by 2050 (O'Neill, 2016). Clearly, the growing specter of antibiotic resistance warrants a reevaluation of long-term infection control strategies for prominent pathogens.

While the pursuit of new antibiotics is a global heath imperative, there is justifiable concern over a research and development enterprise that is narrowly focused upon antibiotic discovery. Given that the efficacy among clinically approved antibiotics is achieved via bacteriostatic or bactericidal mechanisms, extensive use of any given antibiotic therapy will eventually yield resistant populations that emerge as a source of infection (Laxminarayan et al., 2013; Medina and Pieper, 2016). A circumspect approach to infectious disease management mandates the exploration of therapeutic alternatives that are devised to alleviate the selective pressure imposed by antibiotics (Laxminarayan et al., 2013; Medina and Pieper, 2016). Providing a rationale to advance the latter effort, the virulence attributes of many clinically relevant pathogens are regulated through physiological pathways that can be inhibited or ablated without cytotoxic effects. In this way, so-called anti-virulence therapies provide a means of attenuating infectious illness without spurring evolution toward a resistant phenotype (Cegelski et al., 2008; Laxminarayan et al., 2013; Rasko and Sperandio, 2010). Therapeutic targeting of quorum sensing is a paradigmatic anti-virulence strategy that may prove efficacious against some of the most pervasive and problematic bacterial pathogens. Chief among these is *Staphylococcus aureus*, which remains one of the most frequent causes of both hospital and community-acquired infection (Lowy, 1998; Tong et al., 2015).

The propensity of *S. aureus* to acquire antibiotic resistance is evidenced by the reoccurring clinical pattern whereby epidemics caused by resistant isolates emerge rapidly after a new antibiotic is introduced for infection control (Chambers and Deleo, 2009). While *S. aureus* is classified as an opportunistic pathogen, the

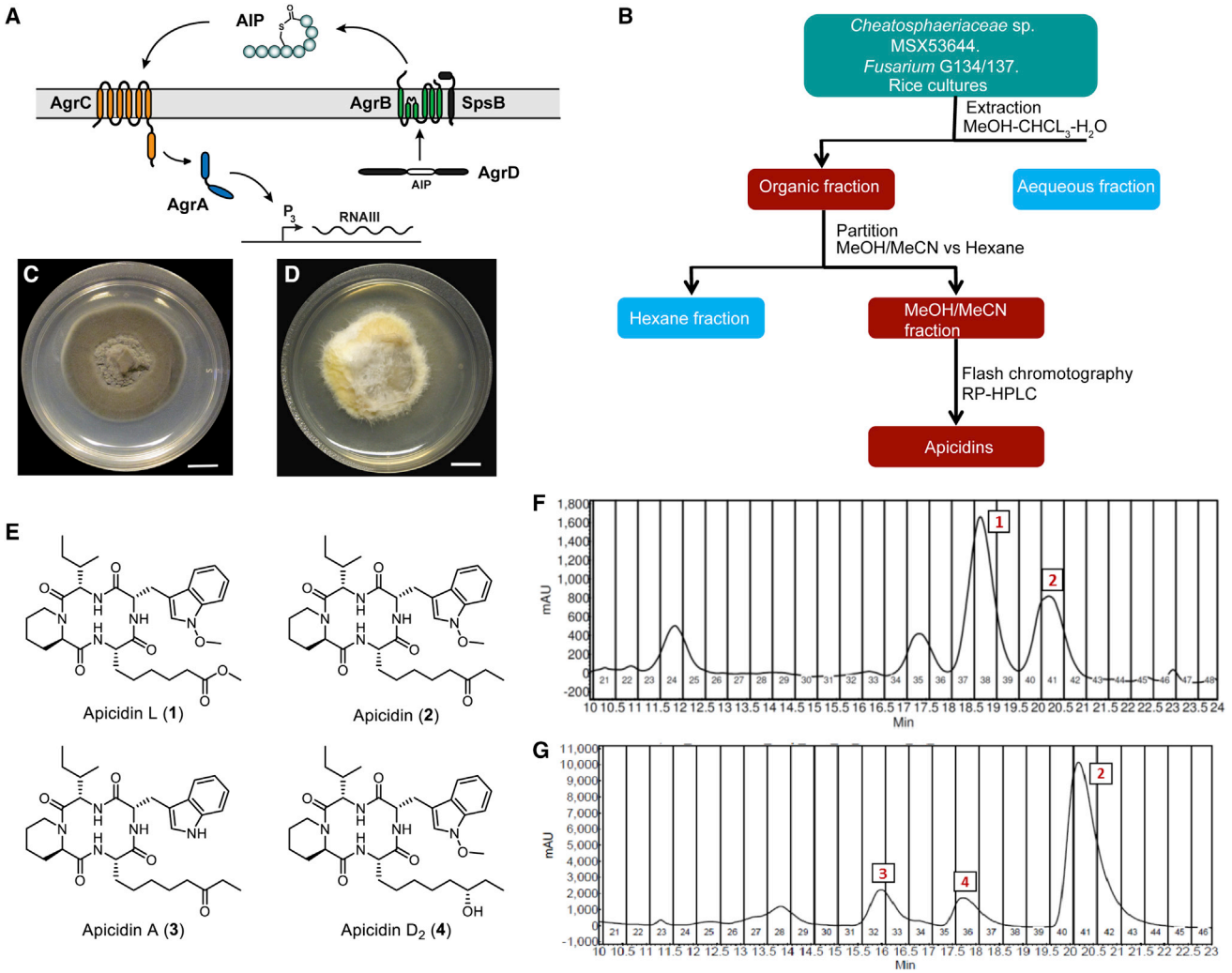

Figure 1. The *agr* System and Isolation of Apicidin

(A) Schematic of the *agr* system.

(B) Flowchart for isolation of apicidins from solid-state culture extracts.

(C) *Chaetosphaeriaceae* sp. (MSX53644) grown on PDA (scale bar, 10 mm).

(D) *Fusarium* sp. (G134 and G137) grown on PDA (scale bar, 10 mm).

(E) Apicidin structures.

(F) Preparative chromatogram (λ = 254 nm) of the fraction used to purify compounds 1 and 2 from MSX53644.

(G) Preparative chromatogram (λ = 254 nm) of the fraction used to purify compounds 2–4 from G134 and G137 (each chromatogram is representative of multiple runs).

capacity of highly aggressive USA300 lineages of methicillin-resistant *S. aureus* (MRSA) to inflict disease among "healthy" community-dwelling individuals has reached pandemic proportions (Chambers and Deleo, 2009; DeLeo et al., 2010; Otto, 2010). The hyper-virulent nature of "community associated" MRSA (CA-MRSA) strains has been attributed to heightened expression of core genome-encoded virulence factors such as α-hemolysin and α phenol soluble modulin (PSMα) peptides, which subvert host defense by exerting cytolytic effects upon immune effector cells (Cheung et al., 2011; Otto, 2010).

Like other *S. aureus* strains, MRSA utilizes quorum sensing to synchronize virulence factor induction in proportion to prevailing cell density (Novick and Geisinger, 2008; Thoendel et al., 2011). Encoded by the *agrBDCA* operon, the quorum-sensing signaling apparatus achieves maximal activity at high cell densities when ambient *agrBD*-derived autoinducing peptides (AIPs) reach a concentration threshold necessary to activate the AgrC-A two component signal transduction system (Figure 1A). There are four different types of AIP signal structures (AIP-I, -II, -III, and -IV), and in turn four types of AgrC receptors, depending on the *S. aureus* strain. The respective ligand receptor interaction between AIP and the sensor histidine kinase AgrC initiates the signaling cascade via phospho-transfer-mediated activation of the response regulator AgrA. The DNA binding capability of

AgrA mediates distinct transcriptional pathways from the systems' two oppositely oriented promoter units (Queck et al., 2008). Whereas the P2 promoter activates an auto-induction circuit via *agrBDCA* expression, the P3 promoter exponentially increases the system's major effector molecule, RNAIII, which regulates >200 virulence factor genes for the purpose of countering host defense and promoting tissue invasion (Kavanaugh and Horswill, 2016; Novick and Geisinger, 2008; Thoendel et al., 2011). Within the context of acute infection, *agr*-regulated quorum sensing coordinates an explosive outburst of virulence factors that are manifestly harmful to the host (Mayville et al., 1999; Wright et al., 2005). As such, the therapeutic potential of quorum-sensing inhibitors (often termed quorum quenchers) has been intensively investigated (Daly et al., 2015; Figueroa et al., 2014; Gordon et al., 2013; Muhs et al., 2017; Nielsen et al., 2014; Quave et al., 2015; Sully et al., 2014; Wright et al., 2005).

The overall goal of the present study was to identify quorum-sensing inhibitors that prove efficacious as anti-MRSA interventions. To this end, we discovered the potent activity of the compound apicidin by screening a library of terrestrial, freshwater, and endophytic fungal metabolites, where apicidin was biosynthesized by fungal strains of terrestrial (MSX53644; *Chaetosphaeriaceae* sp., Chaetosphaeriales, Ascomycota) and endophytic (G134 and G137; *Fusarium* sp., Nectriaceae, Hypocreales, Ascomycota) origins. In a non-bactericidal manner, apicidin-inhibited quorum-sensing activity across *S. aureus* isolates, achieving low micromolar IC_{50}s. Importantly, the translatability of apicidin-mediated *in vitro* activity to efficacy *in vivo* was confirmed in a cutaneous challenge model that also revealed quorum-sensing interference within the infectious environment. Consistent with the latter finding, apicidin treatment enhanced polymorphonuclear neutrophil (PMN) accumulation and function at cutaneous sites of infection. Together, these results indicate that apicidin-mediated inhibition represents a promising strategy to limit MRSA virulence and promote host defense.

RESULTS

Identification of Apicidin and Related Analogs as *S. aureus agr* Inhibitors

The exploration of bioactive natural products has emerged as a promising means of pursuing antimicrobial and anti-virulence leads such as *S. aureus* quorum-sensing inhibitors (Cech and Horswill, 2013; Muhs et al., 2017; Quave and Horswill, 2014; Quave et al., 2015; Todd et al., 2017). This approach recently led to the identification and characterization of ω-hydroxyemodin, an AgrA-antagonizing small molecule derived from the fungus *Penicillium restrictum* (Daly et al., 2015; Figueroa et al., 2014). In the present study, a class of fungal metabolites, termed apicidins, were uncovered through separate screens of both terrestrial and endophytic fungi. The terrestrial strain, MSX53644 (*Chaetosphaeriaceae* sp., Chaetosphaeriales, Ascomycota), was cultivated over rice and subjected to purification (Figure 1B) to yield two cyclic tetrapeptides that were identified using HRESIMS and NMR as the known natural product, apicidin (2), and a new natural product analog of apicidin, which was named apicidin L (1) (Figure 1E). In a parallel analysis, endophytic fungi from medicinal plants were studied. LC-MS analysis of endophytes (G135 and G137), which were isolated from the roots of yerba mansa (*Anemopsis californica* [Nutt.] Hook. and Arn. [Saururaceae]) (Bussey et al., 2015), showed the presence of apicidin by matching retention time, HRESIMS, and tandem mass spectrometry data (El-Elimat et al., 2013) (Figures S1–S3). Considering our interest in this class of compounds, and in an attempt to isolate more structurally related analogs, these samples were further purified using reversed-phase preparative high-performance liquid chromatography (HPLC) to yield more apicidin (2) and two structurally related analogs: apicidin A (3) and apicidin D_2 (4) (Figures 1E–1G).

The bioactivity of apicidin and its analogs were screened via *in vitro* assays that examined the ability of the compounds to suppress *S. aureus agr* activation in a nonbiocidal manner (Quave and Horswill, 2014). Beginning with well-established *agr* P3 reporter based assays, time course experiments measuring the dose effects of apicidin and analogs showed potent activity against all *agr* types with negligible effects upon bacterial growth (Figure 2A; Table S1). Similarly, apicidins' broad suppression of *agr* activation was corroborated in parallel experiments measuring inhibition of red blood cell (RBC) lysis. In all cases, apicidin and analogs mediated *agr* inhibition at IC_{50} values in low micromolar concentrations that were sub-inhibitory for growth. Interestingly, *agr* types II and IV represented the most sensitive and resistant alleles to apicidins' impact, respectively. Relative to its analogs, apicidin (2) showed the most impressive actions as an *agr* inhibitor (Figure 2), and, therefore, became the focus of our subsequent efforts to evaluate its efficacy as a nontoxic, pan inhibitor of *agr* activation. Further corroboration of the broad inhibitory effects of this compound on a per cell basis was demonstrated via flow cytometry using the same *agr* P3 reporter strains (Figure S4).

To evaluate the impact of apicidin on global transcriptional regulation, we conducted RNA-seq analysis upon USA300 MRSA wild-type (WT) cultures grown in the presence of apicidin or vehicle control. For purposes of comparing the effects of apicidin on the MRSA transcriptome to those of an *agr* null, we performed parallel RNA-seq analysis of the WT and Δ*agr* preparations. Using a 4-fold cutoff as the threshold for differential gene expression, we found that apicidin altered the expression of thirty genes, with many of these representing prototypical *agr* targets, such as *hla*, *RNAIII*, *psmα*, and *spl* genes (Figure 2B; Table S2). Together, these data corroborate and extend upon the inhibitory capability of apicidin by demonstrating a transcriptional signature that is largely confined to *agr*-regulated transcripts, and most impressively suppressive against cytolytic toxin induction (Figure 2B). Congruent with the apicidin-induced inhibition of *agr*-regulated virulence factors, we observed enhanced whole blood killing of MRSA when bacteria were cultured in the presence of apicidin prior to inoculation (Figure 2C).

Next, we conducted a series of *in vitro* assays to systematically assess the relative contribution of each of the core genetic elements of the *agrBDCA* operon (Figure 1A). The membrane-embedded peptidase AgrB is responsible for the first step, by processing the AgrD pro-peptide into the functional,

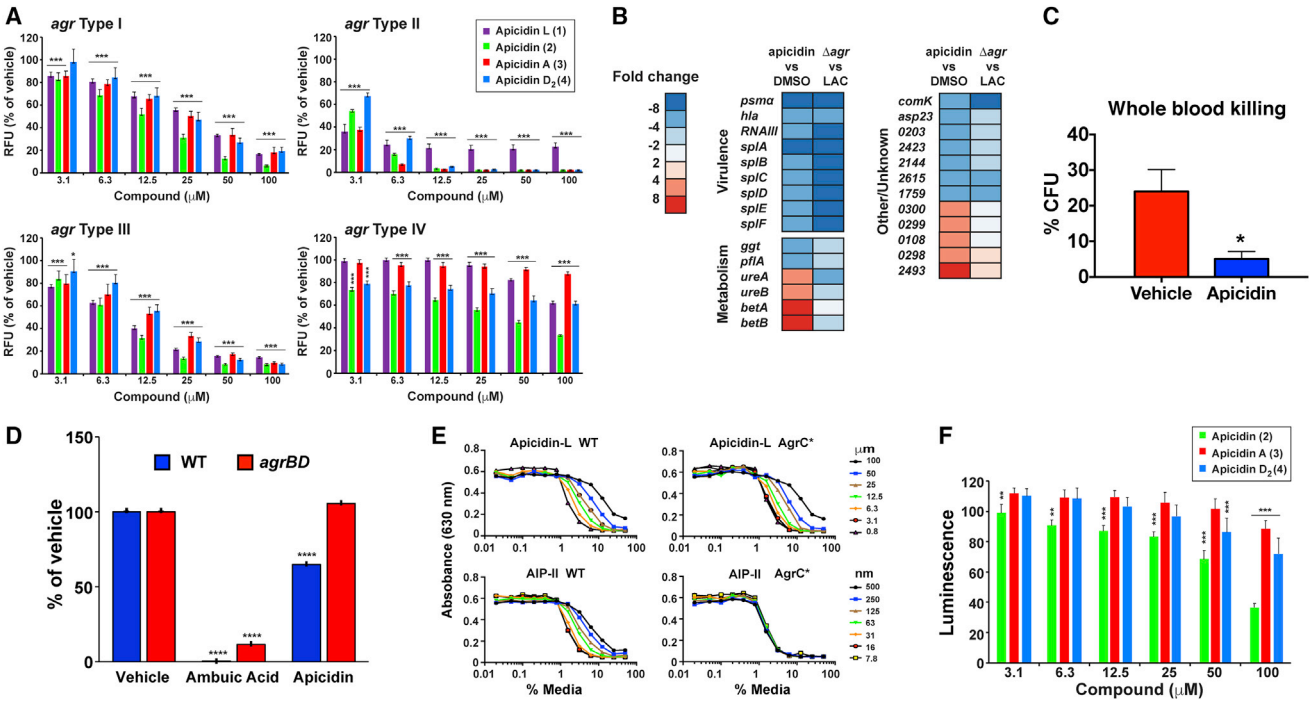

Figure 2. Apicidin Inhibits MRSA *agr* Function by Targeting AgrA

(A) Apicidin (apicidin L, apidicin, apicidin A, apicidin D_2) mediated suppression of *agr*-P3 reporters (inhibition extends to all four *agr* types). Post-test *p < 0.05, **p < 0.01, and ***p < 0.005; n = 10.

(B) USA300 MRSA LAC genes showing >4-fold change in expression after treatment with 100-μM apicidin versus DMSO vehicle control (n = 3), determined using RNA sequencing (RNA-seq). For comparison, gene expression was also measured in the *agr* mutant treated with DMSO. Numbers for genes of unknown function correspond to locus tags SAUSA300_XXXX.

(C) Heparinized human whole blood was inoculated with MRSA organisms cultured (4 h) in the presence of 100-μm apicidin or vehicle (n = 8). After 1 h, CFUs from inoculated whole blood were plated out and compared with the starting inoculum and reported as percent killing. Error bars represent SEM. Post-test *p < 0.05.

(D) Mass spectrometric measurements comparing ambuic acid and apicidin's impact on AIP levels in MRSA WT (blue bars, labeled WT) and constitutive AIP-producing (red bars, labeled *agrBD*) strains. Each compound was tested at 100-μM concentration (n = 3). Statistical analysis was performed using the Student's t test, ****p < 0.001.

(E) Effect of increasing concentrations of apicidin L on reporter strains for WT AgrC versus constitutive AgrC*. Apicidin L is compared to the AIP-II inhibitor control (representative; also performed with same results on apicidin, n = 3).

(F) Effect of increasing concentrations of apicidin, apicidin A, and apicidin D_2 on P3-*lux* reporter activation using an *agr* null strain containing an *agrA* plasmid (n = 4). Post-test *p < 0.05, **p < 0.01, and ***p < 0.005.

extracellular AIP signal. To determine if apicidin inhibits *agr* function at the level of AIP signal generation, we used an established system whereby AIP is constitutively produced in an engineered USA300 MRSA strain (Todd et al., 2017). This engineered strain (labeled *agrBD*) decouples AIP signal biosynthesis from quorum-sensing regulation, enabling quantitative mass spectrometric analysis of culture supernatants to determine AIP levels (Figure 2D). An inhibitor that targets AgrB or another aspect of AIP signal biosynthesis is expected to prevent AIP production in both WT and engineered *S. aureus* strains, while an inhibitor targeting another competent of the *agr* system would only prevent AIP production in the WT strain. Consistent with these predictions, ambuic acid, a known *agr* signal biosynthesis inhibitor (Todd et al., 2017), significantly inhibited AIP peptide production by both strains. In contrast for apicidin, the WT strain was significantly inhibited by 35%, while no statistically significant inhibition was observed for the constitutive AIP-producing strain (Figure 2D). The results of these experiments suggest that apicidin does not target AgrB function or the signal biosynthesis process in general.

Next, we explored the possibility that apicidin interferes with the sensory activity of AIP receptor AgrC. Toward this goal, we employed an R238H construct bearing a point mutation that confers constitutive AgrC activity (Daly et al., 2015; Geisinger et al., 2009), and thereby enables phosphoactivation of AgrA to occur independently of AIP binding. With a hemolysis readout, apicidin L (1) imposed a dose-dependent inhibition of lytic activity on AgrC R238H that mirrored the response of AgrC WT (Figure 2E). In contrast, treatment with noncognate AIP-II, which competitively binds and inhibits AgrC function (Gordon et al., 2013), had no impact on AgrC R238H activation as expected. These results suggest that apicidin mediates its effects downstream of AgrC activation.

Finally, we set out to determine if AgrA serves as the target of apicidin. To this end, we employed an *agr* P3 *lux* reporter,

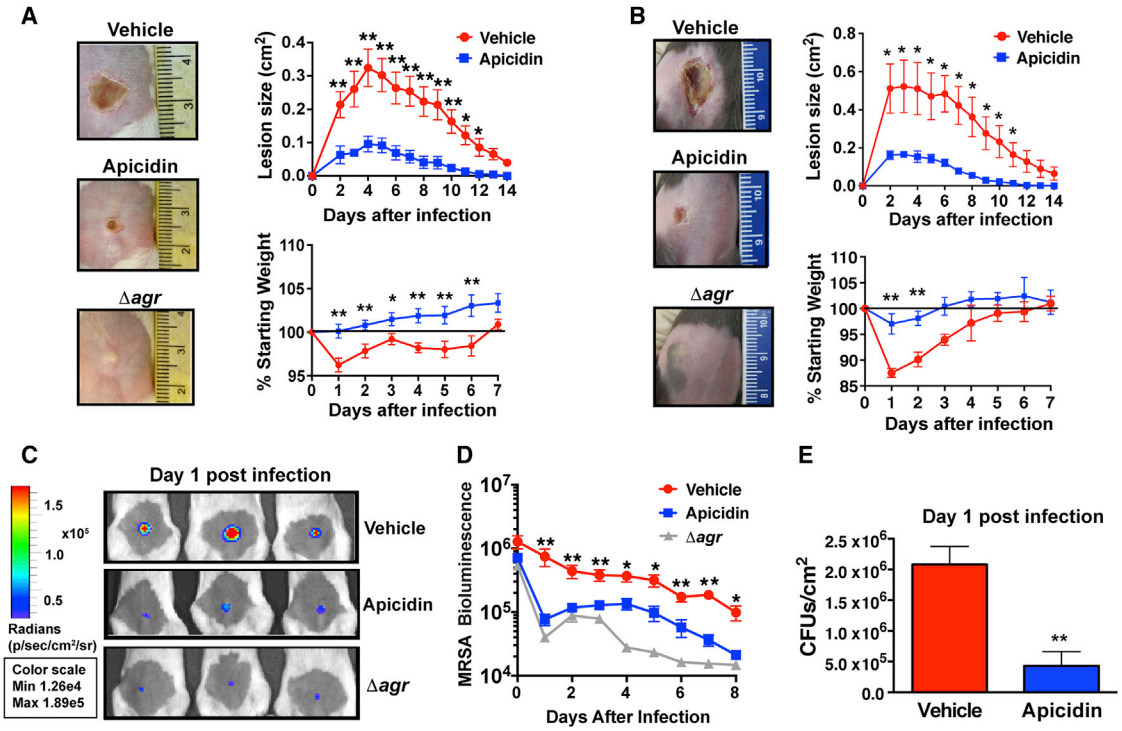

Figure 3. Apicidin Abates MRSA Pathogenesis

(A and B) Representative images of tissue injury following infection with MRSA WT or Δ*agr* mutant (±5 μg apicidin) and corresponding skin lesion size and weight loss and measurements following infection for the indicated groups in BALB/c (n = 20) (A) and C57BL/6 mice (n = 5) (B). Error bars represent SEM. Post-test *p < 0.05 and **p < 0.01.

(C) Representative images showing decreased bacterial burden in apicidin-treated animals relative to Δ*agr* or vehicle controls 1 day after intradermal challenge with 2 × 10^7 CFUs MRSA Lux$^+$ or its *agr* null counterpart.

(D) Corresponding noninvasive, longitudinal measurements of bioluminescence following skin infection with MRSA Lux$^+$ or Δ*agr* Lux$^+$ (n = 8).

(E) CFUs recovered from BALB/c skin lesions 1 day after infection (n = 5).

where bioluminescence can only be achieved with expression of AgrA (Sully et al., 2014). The dose-dependent inhibition of *agr*-P3-driven bioluminescence shows that apicidin specifically interferes with AgrA-dependent quorum-sensing activation (Figure 2F). Considering the strain used is *agr* type I, apicidin (2) worked the best, while apicidin A (3) and D_2 (4) were less effective, but still significantly inhibited. Taken together, these mechanistic studies provide compelling evidence that AgrA serves as the molecular target of apicidin.

Apicidin Abates MRSA Pathogenesis

S. aureus causes 76% of skin infections (Moran et al., 2006), more than any other infectious agent. Having demonstrated apicidin's potent quorum-sensing inhibition *in vitro*, we next investigated the translatability of this activity within a relevant infectious context *in vivo* during skin infection using approaches developed by our group (Muhs et al., 2017; Paharik et al., 2017; Todd et al., 2017). For this purpose, an intradermal challenge model was employed by delivering a single 5-μg dose of apicidin as part of the MRSA inoculum suspension. To assess the contribution of differential immune skewing of the host to any apicidin-induced effects, we employed both C57BL/6 and BALB/c mice in our initial challenge experiments. Irrespective of murine strain background, apicidin treatment significantly reduced skin ulceration size and weight loss following MRSA challenge (Figures 3A and 3B). Together, these data show that when applied as an anti-infective, apicidin impressively attenuates MRSA-induced disease following MRSA challenge.

To determine the impact of apicidin on cutaneous bacterial burden, challenge experiments were conducted with a MRSA Lux+ strain and compared against analogous challenges with its *agr* deletion construct Δ*agr* Lux$^+$. An advantage of this approach is the noninvasive and longitudinal manner with which bacterial burden can be measured. While an apicidin-induced decrease in bacterial burden was observed throughout the experiment, this effect was most impressively evident one day following infection, where it closely approached values obtained after Δ*agr* Lux$^+$ challenge (Figures 3C and 3D). Corroborating the apicidin-mediated enhancement of bacterial clearance via IVIS imaging, significantly fewer CFUs were recovered from lesional skin one day after infection in apicidin treated mice relative to controls (Figure 3E). In addition, parallel analysis of lesion development in the same apicidin and control mice showed a correspondence between MRSA-driven bioluminescence and dermatopathology.

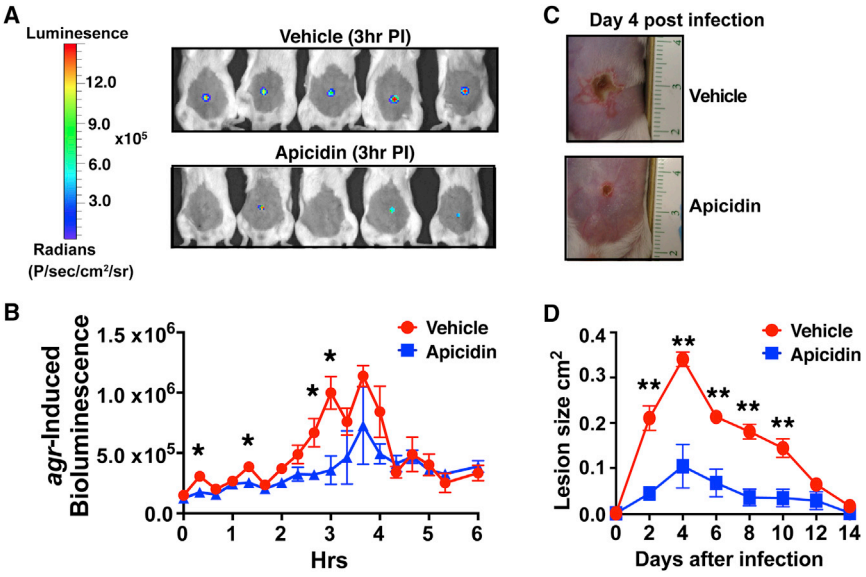

Figure 4. Apicidin-Mediated Quorum-Sensing Inhibition Corresponds with Attenuated Skin Injury

(A) Images of *agr*-P3 reporter activity (bioluminescence) 3 h post infection (±5 μg apicidin).

(B) Kinetics of *agr* activation in apicidin and vehicle-control-treated mice after infection (n = 5).

(C) Representative images of apicidin or control groups at the indicated time points after infection (n = 5).

(D) Skin lesion size measurements at the indicated time points after infection. Error bars represent SEM. Post-test *p < 0.05 and **p < 0.01.

Apicidin Mediates Quorum Quenching at *In Vivo* Sites of Infection

Having demonstrated that apicidin attenuated MRSA-induced illness (e.g., tissue damage, weight loss, bacterial burden), we set out to determine if these therapeutic effects corresponded with quorum-sensing interference *in vivo*. Based on previous work by Wright et al., which showed that the extent of *S. aureus*-induced dermatopathology is proportional to the magnitude of *agr* activation during the first 4 h of infection (Wright et al., 2005), we selected this key time period for in-depth analysis of the apicidin impact against multiple *agr* types *in vivo*. By challenging mice with an *agr*-P3 lux reporter strain and monitoring the early kinetics of *agr* activation, we showed that the attenuation of MRSA virulence in apicidin-treated animals occurred alongside a significant interference of *agr* activation *in vivo* (Figures 4A and 4B). To further demonstrate that the level of *agr* interference mediated by apicidin corresponded with a hypo-virulent infectious phenotype, we measured the ensuing skin ulcers in these animals over a 14-day period and found a dramatic reduction in cutaneous injury in apicidin-treated animals (Figures 4C and 4D). Altogether, these data demonstrate that the apicidin-mediated attenuation of MRSA pathogenesis corresponds with quorum-sensing inhibition both *in vitro* and *in vivo*.

In Vivo Efficacy of Apicidin Extends to *agr* Type-II Isolates

We next set out to investigate the potential of apicidin to show broad spectrum *in vivo* efficacy against multiple *S. aureus agr* types. To this end, the capacity of apicidin to influence the infectious outcome following intradermal challenge with a USA100 MRSA, *agr* type II, invasive isolate was assessed. As observed in analogous challenge experiments with *agr* type I strains, apicidin-treated animals exhibited significant attenuation in USA100-induced dermonecrotic injury relative to controls (Figures 5A and 5B). By engineering an *agr* P3-lux reporter into this *agr* type II isolate, we showed that the protective effects of apicidin treatment against multiple *agr* types corresponds with real-time quorum quenching at the cutaneous challenge site (Figures 5C and 5D). Carrying out the P3-lux-infected animals further corresponded with a significant reduction in lesion size at day 4 (Figure 5E), demonstrating the importance of early intervention in *agr* signaling with the different USA100 lineage.

Apicidin Treatment Enhances PMN Responses after MRSA Skin Challenge

Given that apicidin exposure is nontoxic to MRSA *in vitro*, the impressive decrease in MRSA burden observed during *in vivo* infection could be a function of enhanced staphylocidal host immune responses. The recruitment of PMNs to sites of cutaneous *S. aureus* infection is critical for pathogen clearance (Miller and Cho, 2011; Spaan et al., 2013). Abundant in the circulation, PMNs orchestrate protective anti-*S. aureus* cutaneous immune responses by extravasating through vascular endothelium proximal to infectious foci where they sequentially accumulate, phagocytose, and clear *S. aureus* organisms (Spaan et al., 2013). By performing challenge experiments with MRSA GFP$^+$, we were able to show that the apicidin-induced attenuation of MRSA injury and burden corresponded with an increase in the number of phagocytic PMNs accumulating at cutaneous challenge sites (Figure 6A). The frequency of MRSA uptake was unaltered between apicidin and vehicle-exposed PMNs, which matched control experiments that showed no significant impact of apicidin on PMN function (Figure S5). Nonetheless, there was an aggregate increase in the phagocytic capacity of the entire PMN infiltrate during infection with the apicidin-treated group (Figure 6A). Furthermore, the apicidin-induced increase in PMN infiltration was even further surpassed in the setting of *agr* null challenge, revealing an inverse proportionality between the magnitude of *agr* activity and the strength of the ensuing PMN response. Meanwhile, the lack of an effect on cutaneous PMN infiltration following mock challenge indicates that apicidin's impact on PMN responses during infection are largely a consequence of *agr* interference (Figure 6B).

To explore the possibility that apicidin exposure increases the resistance of host cells to *agr*-regulated virulence factors, we examined the prophylactic effects of apicidin administration

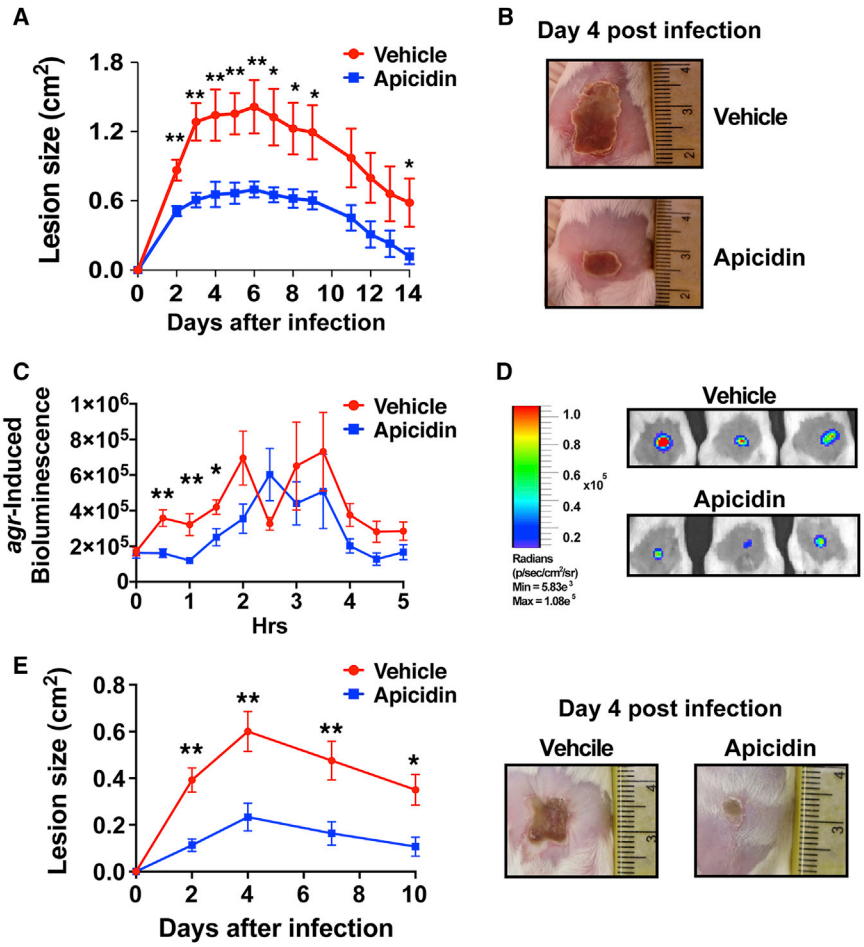

Figure 5. Apicidin-Mediated Attenuation of MRSA Pathogenesis and *In Vivo* Quorum Quenching Observed against Multiple *agr* Types

(A) Skin lesion measurements following infection with 2 × 10^7 CFUs of an *agr* type-II invasive USA100 MRSA isolate (±5 μg apicidin). Error bars represent SEM. Post-test *p < 0.05 and **p < 0.01 (n = 5).

(B) Representative images of tissue injury following infection with *agr* type-II ± apicidin.

(C) Kinetics and representative images (1-h time point; right) of *agr*-P3-induced bioluminescence after intradermal challenge with 1 × 10^7 CFUs of an *agr* type-II P3-lux reporter (± apicidin; n = 5). Error bars represent SEM. Post-test *p < 0.05 and **p < 0.01.

(D) Corresponding skin lesion size measurements at the indicated time points following infection with strain described in (C) (n = 8). Error bars represent SEM. Post-test *p < 0.05 and **p < 0.01.

(E) Representative images of tissue injury (day 4) following infection with *agr* type-II reporter described in (C).

against sterile challenge with cytotoxin-containing MRSA supernatants. The similar degree of dermonecrotic injury sustained by apicidin and control groups following MRSA intoxication suggests that apicidin's ability to attenuate infectious injury is principally achieved by limiting host cell exposure to *agr*-induced virulence factors (Figure 6C). In view of the correlation between MRSA-induced disease attenuation and cutaneous PMN accumulation, we investigated the dependence of apicidin's therapeutic effects upon the latter. To this end, we depleted host PMNs via administration of an anti-Ly6G antibody on both the day prior to and the day of infection. The equivalent severity of skin ulceration and bacterial burden within the context of neutropenia demonstrates that apicidin's therapeutic efficacy requires a functional PMN compartment (Figure 6D). Taken together, these findings indicate that the capacity of apicidin to bolster host defense and improve disease outcome was largely a by-product of *agr* inhibition, which in turn sensitizes MRSA for PMN-mediated phagocytic clearance.

To better understand the mechanistic basis of the apicidin-induced increase in PMN density at cutaneous sites of infection, we assessed the cytokine milieu of lesional tissue one day after infection. Interestingly, the apicidin-induced increase in cutaneous PMNs did not correspond with a commensurate increase in prototypical PMN chemoattractant or granulopoiesis factors. In fact, preparations from apicidin-treated animals showed a decrease in the production of CXCL-1 and granulocyte-colony stimulating factor (G-CSF) relative to controls, suggesting that apicidin's ability to boost PMN responses does not occur as a result of alleviating a MRSA-induced strain upon factors that mediate extravasation into infected tissue (Figure 7A). In further support of this, equivalent cutaneous endothelial cell recovery and PMN abundance in the peripheral blood (PB) was observed between apicidin-treated and control mice (Figure 7B). While similar PMN counts in the skin-draining lymph nodes (LNs) suggests that altered trafficking to alternative sites known to harbor PMNs after skin infection plays little role in the apicidin-induced increase in cutaneous PMN accumulation (Figure 7C). Together, these data suggest apicidin's capacity to enhance PMN infiltration is chiefly the result of alterations within the infectious microenvironment.

Given that extraordinary expression of *agr*-regulated cytolytic toxins is a defining feature of USA300 MRSA-induced disease, we explored apicidin's impact upon PMN persistence within the infectious environment. Because PMN apoptosis-efferocytosis is the cellular fate that is most advantageous to the host, it was important to distinguish the rate of cell death between PMNs that are actively executing the effector function of MRSA uptake (GFP^+) and those that have not. To this end, we assessed the frequency of PMNs in late stage apoptosis-necrosis within lesional skin preparations of MRSA GFP^+ challenged mice. For the phagocytic and non-phagocytic PMNs, we observed an apicidin-induced decrease in the frequency of PI^+, late-stage apoptotic-necrotic cells (Figure 7D), although

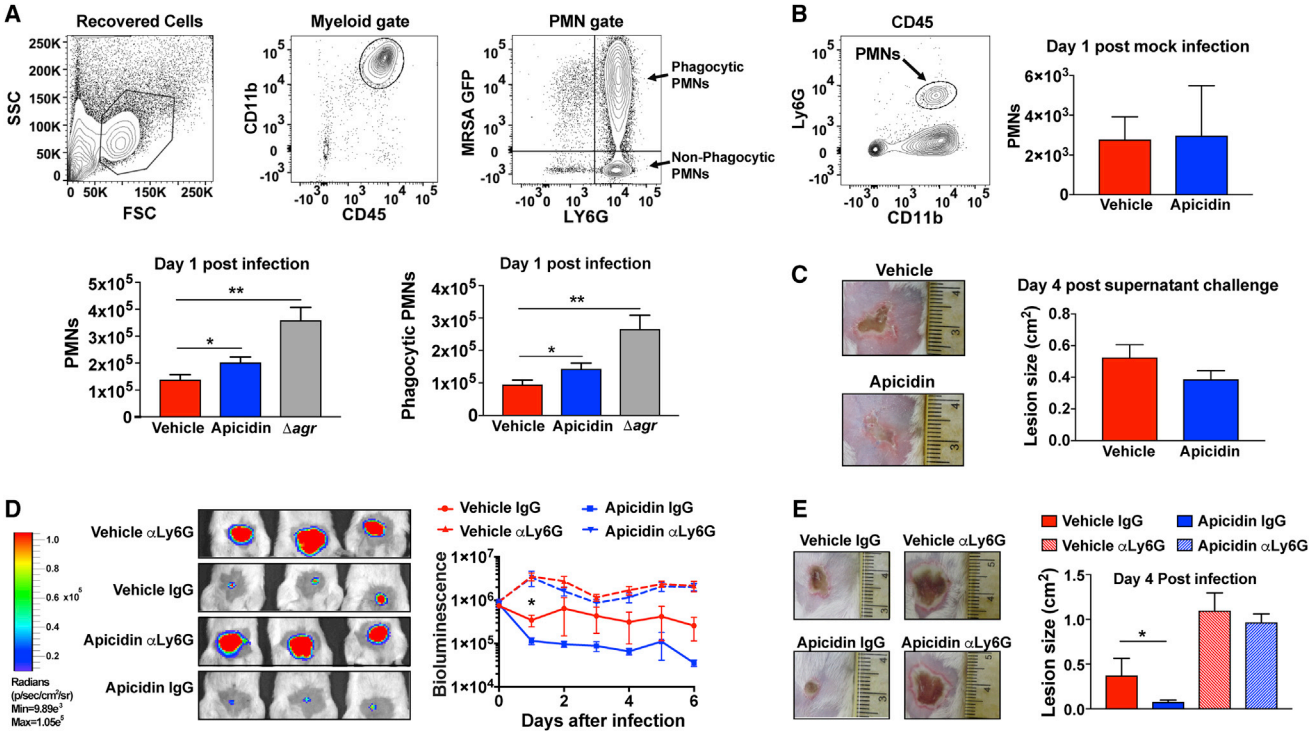

Figure 6. Apicidin Treatment Enhances PMN Responses after MRSA Skin Challenge

(A) Gating strategies (top) for identification of PMNs recovered from lesional skin and corresponding PMN accumulation values (bottom) 1 day after intradermal challenge with 2 × 10^7 MRSA WT expressing GFP (± apicidin) or its *agr* null counterpart (n = 8). Error bars represent SEM. Post-test *p < 0.05 and **p < 0.01.

(B) Gating strategy (left) and enumerated PMNs (right) 1 day after intradermal saline challenge (± apicidin; n = 8).

(C) Representative skin injuries 4 days after sterile challenge (intradermal) with 30 μL of WT MRSA supernatant at the skin sites intradermally inoculated with saline (± apicidin) 3 h prior (n = 6).

(D) Representative bioluminescence images 1 day after intradermal challenge (2 × 10^7 CFUs MRSA Lux$^+$) among apicidin-treated and control groups receiving 100 μg of the PMN-depleting anti-Ly6G antibody or isotype control via intraperitoneal injection administered both the day prior and the day of infection. Corresponding time course values (right) of MRSA burden for the indicated groups (n = 6).

(E) Representative images of skin injury (left) and corresponding lesion size measurements 4 days after infection for the indicated groups (n = 5). Error bars represent SEM. Post-test *p < 0.05 and **p < 0.01.

not quite to the same level as the *agr* mutant. Together, these data suggest that apicidin impacts the host-pathogen interface by suppressing *agr*-regulated virulence factors, especially immune cell lysing toxins, and thereby extends cytoprotective effects upon cutaneous PMNs.

DISCUSSION

Since the advent of antibiotic therapy, *S. aureus* has evolved resistance to every frontline antibiotic used in healthcare settings and done so with devastating human health effects. Considering that ancestral *S. aureus* is highly sensitive to virtually every antibiotic ever devised, the broad resistance features of today's most pervasive and problematic isolates suggest that modern medicine's reliance on antibiotic therapy has spurred resistance development (Chambers and Deleo, 2009; DeLeo and Chambers, 2009; Spellberg et al., 2015). Pandemic CA-MRSA provides an illustrative example of how infectious transmissibility brought on the concurrent evolution of antibiotic resistance and hyper-virulence (Cheung et al., 2011; Otto, 2010). Considering that MRSA is already one of the most pervasive and problematic causes of bacterial infection, the continuation of such trends poses a serious threat to public health and highlights the need for new treatments. Through quorum-sensing inhibition and immune boosting, apicidin treatment offers a therapeutic strategy to sensitize MRSA to host-mediated clearance in a resistance-avoiding fashion.

Herein, we report efficacious application of apicidin as an anti-virulence agent. Apicidin's activity as a pan-quorum-sensing inhibitor was confirmed via assays that demonstrated suppression of *agr* activation of all types in a non-biocidal manner. Further evidence of *agr* interference was achieved via RNA-seq analysis, showing that the majority of apicidin-affected transcripts were *agr*-regulated and included the prototypical cytolytic toxins *hla* and *psms*. To determine the apicidin target within the *agr* machinery, assays specific to each component were employed, surprisingly narrowing the activity to AgrA (Figure 2). Based on the cyclic peptide-like nature of the apicidin structure (Figure 1), we anticipated that the AgrC receptor would be the target, in similar fashion to synthetic AIP derivatives (Gordon et al., 2013, 2016). However, the ability of apicidin to definitely inhibit the constitutive AgrC R235H construct, and also prevent AgrA

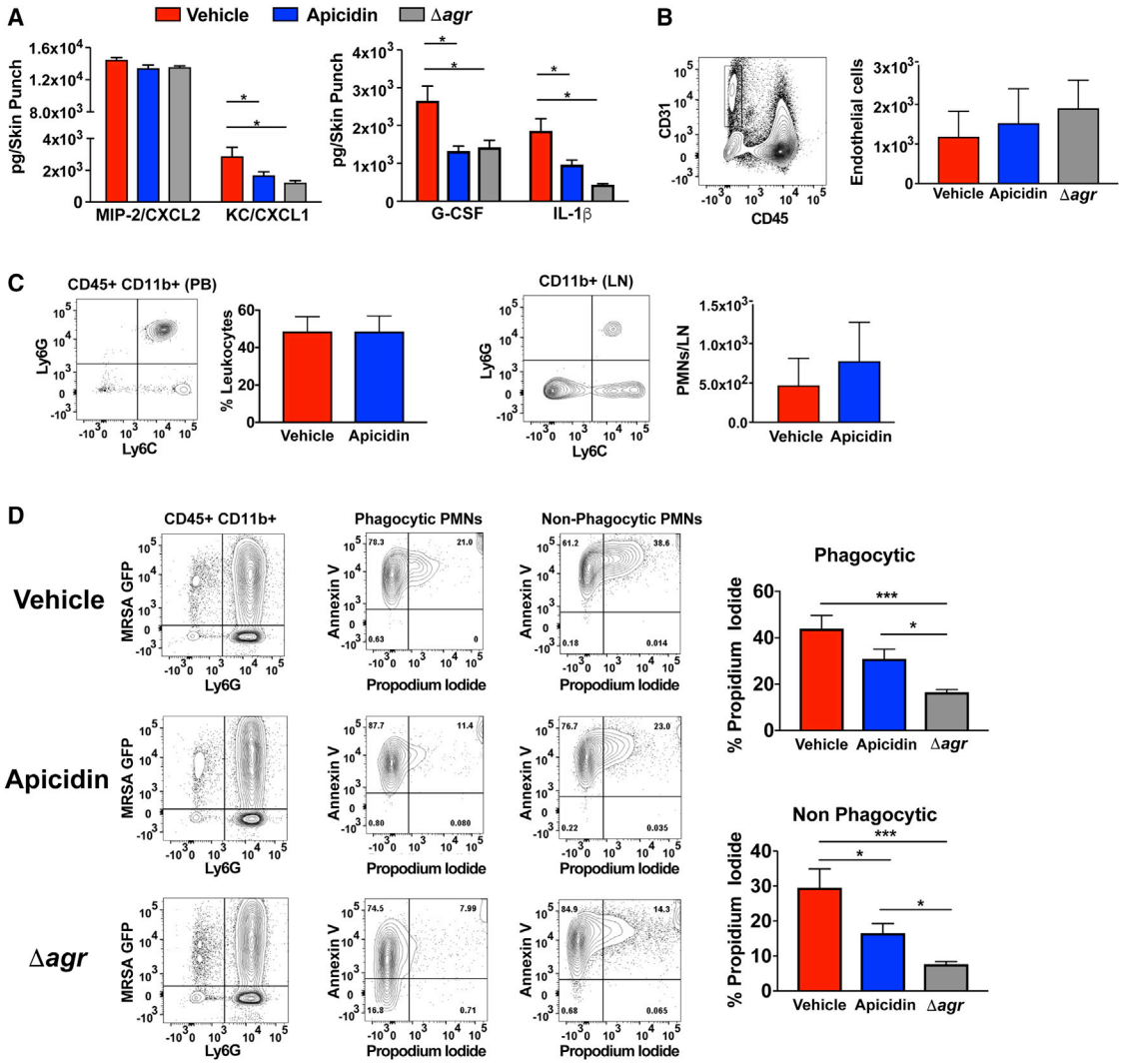

Figure 7. Apicidin Confers Cytoprotective Effects upon Skin-Infiltrating PMNs after MRSA Skin Challenge

(A) Supernatants from skin tissue homogenates were collected 1 day after infection and subjected to cytokine array analysis (n = 6).

(B) Gating strategies (left) and enumeration of (right) $CD31^+$ $CD45^-$ endothelial cells recovered from lesional tissue 1 day following MRSA challenge (± apicidin) or its *agr* null counterpart (n = 6).

(C) Gating strategies (left) and enumeration of PMNs (right) in PB and skin-draining LNs 1 day after MRSA skin challenge (n = 6).

(D) Gating strategies (left) and corresponding frequency values (right) for propidium $iodide^+$ phagocytic (GFP^+) and non-phagocytic (GFP^-) PMNs recovered from skin lesions 1 day after intradermal challenge with 2×10^7 MRSA GFP^+ (± apicidin) or its *agr* null counterpart (n = 5). Error bars represent SEM. Post-test *$p < 0.05$ and ***$p < 0.001$.

activation of a P3-lux reporter, strongly indicated that AgrA is the actual target. Thus, apicidin joins savarin and ω-hydroxyemodin (which is another fungal metabolite) as the known AgrA inhibitors (Daly et al., 2015; Sully et al., 2014). Additional work will be required to identify the precise AgrA residue(s) that is required for its interaction with apicidin and to further define the mechanism of apicidin inhibition.

The translatability of apicidin's *agr* inhibitory activity to *in vivo* therapeutic efficacy was confirmed using a MRSA intradermal challenge model. As a single-dose intervention, apicidin ameliorated multiple measures of clinical disease severity. While a number of *agr* inhibitors have shown the ability to attenuate cutaneous ulcer formation following MRSA challenge (Daly et al., 2015; Mayville et al., 1999; Muhs et al., 2017; Quave et al., 2015; Sully et al., 2014), apicidin is first to show that its efficacy extends to multiple *agr* types using infection models, demonstrating its broad utility as an anti-infective agent. Although, *agr* type-I alleles, which encompass USA300 isolates, are the most pervasive and problematic clinically (Chambers and Deleo, 2009; DeLeo et al., 2010), other *agr* types represent a source of human disease (Tong et al., 2015). For instance, isolates bearing *agr* type-II alleles are the leading cause of hospital-acquired MRSA infection (Limbago et al., 2009). Thus, the applicability of any quorum-targeting therapy is extended by its capacity

to inhibit multiple *agr* types. Consistent with the attenuation of dermonecrotic injury, the single-dose efficacy of apicidin corresponded with significant *agr* interference within the *in vivo* infectious environment following cutaneous challenge with both type-I and type-II MRSA isolates. As previously demonstrated by Novick's group (Wright et al., 2005), the explosive activation of the *agr* system occurring within the first few hours of *in vivo* infection largely dictates the severity of MRSA-induced disease. Consistent with this, we recently showed that the potent *agr* antagonism of *S. caprae*-derived AIP had only a minor benefit as treatment for established MRSA skin infection (Paharik et al., 2017). With this in mind, pharmacologically abating MRSA pathogenesis via quorum-sensing inhibition will require targeting *agr* activity during a narrow temporal window that can ensue rapidly after tissue penetration. Thus, it appears that as a potential clinical intervention, the application of apicidin is best suited as a prophylactic agent.

MRSA is a major contributor to the ever-escalating threat of antibiotic resistant bacterial pathogens. Among the core strategic approaches of the National Institutes of Allergy and Infectious Diseases' antibacterial resistance program are the development of (1) anti-virulence strategies that disarm without directly killing bacteria and (2) immunological interventions that enhance host defenses. The present study demonstrates that these paradigms are complementary in the coordination of host defense, namely, the enhanced effector functionality within the cutaneous PMN network. Both clinical and experimental findings concordantly suggest that the staphylocidal functions of skin-infiltrating PMNs are essential for protective anti-*S. aureus* immunity (Miller and Cho, 2011; Spaan et al., 2013), in contrast to steady-state skin, which is largely devoid of PMNs. Infectious injury activates cytokine-chemokine circuits that in turn forge an inflammatory milieu replete with PMN recruitment, survival, and differentiation factors. Within the context of *S. aureus* skin infection, local production of the quintessential inflammatory mediator IL-1β incites cytokine-chemokine pathways that underlie PMN recruitment and function (Miller and Cho, 2011; Spaan et al., 2013). While IL-1β is clearly required for *S. aureus* host defense, the results from the present study show that increased IL-1β output (as observed in control groups) does not necessarily yield commensurate gains in cutaneous PMNs (Figures 6 and 7). In fact, PMN numbers were greatest in *agr*-null-challenged tissue where IL-1β production was the lowest. These findings suggest that protective anti-MRSA effector responses may be optimal in conditions where local inflammation is finely tuned. Consistent with this notion, apicidin treatment augmented cutaneous PMN responses and hastened MRSA clearance, while subduing inflammatory cytokine production. The inverse relationship between PMN accumulation and the bacterial burden resulting from apicidin treatment is reminiscent of prior work demonstrating the therapeutic efficacy of *S. caprae* AIP. Using a similar model of intradermal challenge, Paharik and Parlet et al. showed that one of the most striking alterations imposed upon the host-pathogen interface via pharmacological targeting of MRSA quorum sensing is increased PMN amassment at sites of infection (Paharik et al., 2017). The present study further clarifies the mechanistic basis for this occurrence by showing that quorum-sensing inhibition confers cytoprotective effects to skin-infiltrating PMNs. When viewed together, these results are consistent with the following interpretation: By disabling *S. aureus* quorum sensing, the resultant suppression of immune-toxigenic virulence factors (e.g., PSMs and α-toxin) increases the survival of PMN effectors that mediate pathogen clearance, the manifestations of which are attenuated tissue damage and accelerated bacterial clearance.

In conclusion, we report the efficacious application of the fungal derivative apicidin as an anti-virulence intervention against MRSA-induced disease. As the threat posed by antibiotic-resistant pathogens continues to grow, there is an urgent need for innovative approaches that are mechanistically distinct from conventional antibiotic therapy, and are tailored for the pathophysiology of specific infectious agents. Apicidin exemplifies such a pioneering treatment modality. By inhibiting virulence factor expression, apicidin impacts host-pathogen interactions in a manner that favors immune clearance of the pathogen and blocks disease progression.

STAR★METHODS

Detailed methods are provided in the online version of this paper and include the following:

- KEY RESOURCES TABLE
- CONTACT FOR REAGENT AND RESOURCE SHARING
- EXPERIMENTAL MODEL AND SUBJECT DETAILS
  - Bacterial strains and plasmids
  - Mice
  - Plant material
  - Fungal strains
- METHOD DETAILS
  - Quenching assays with reporter strains:
  - Hemolytic activity
  - Mass Spectrometric Measurements of AIP
  - Fermentation, extraction and isolation
  - Fermentation, extraction and isolation of compounds from strains G134 and G137
  - NMR methods
  - *S. aureus* skin infections
  - Measurement of quorum quenching *in vivo*
  - Evaluation of skin and blood immune cells
  - Whole blood killing assays
  - RNA Seq
  - Flow cytometry
  - Cytokine Measurements from Tissue Homogenates
- QUANTIFICATION AND STATISTICAL ANALYSIS
  - Statistics
- DATA AND SOFTWARE AVAILABILITY

SUPPLEMENTAL INFORMATION

Supplemental Information can be found online at https://doi.org/10.1016/j.celrep.2019.03.018.

ACKNOWLEDGMENTS

C.P.P. was supported by NIH T32 Training Awards AI007511 and AI007343. A.R.H. was supported by a merit award (I01 BX002711) from the Department

of Veteran Affairs and by NIH Public Health Service Grant AI083211 (Project 3). H.A.C. was supported by NIH T32 AI007511 and American Heart Association Postdoctoral Fellowship 15POST25720016. The libraries of fungal extracts and pure compounds were assembled with partial support from the North Carolina Biotechnology Center (2015-BRG-1208). The authors thank the flow cytometry, microscopy, and genomics core facilities at the University of Iowa for technical assistance, as well as Michael Shay for his technical assistance with the collection of cytokine measurements from infected skin. Mass spectrometric data were collected in the Triad Mass Spectrometry Facility at the University of North Carolina at Greensboro. The authors also thank Dr. Ronan Carroll for providing an annotated USA300 genome for RNA-seq analysis and Dr. Daniel Diekema for providing strains.

AUTHOR CONTRIBUTIONS

C.P.P., J.S.K., H.A.C., T.E.-E., D.A.T., N.B.C., N.H.O., and A.R.H. conceived and designed the experiments. C.P.P., H.A.C., J.S.K., T.E.-E., H.A.R., and D.A.T. performed the experiments. C.P.P., J.S.K., H.A.C., T.E.E., H.A.R., D.A.T., N.B.C., N.H.O., and A.R.H. analyzed the data. C.P.P., H.A.R., C.J.P., N.B.C., N.H.O., and A.R.H. contributed reagents and materials. C.P.P. and A.R.H. wrote the paper.

DECLARATION OF INTERESTS

The authors have no financial or competing interests to declare. A patent has been filed by A.R.H., J.S.K., C.P.P., T.E.E., and N.H.O. on the biological activity of apicidin.

Received: April 10, 2018
Revised: January 27, 2019
Accepted: March 5, 2019
Published: April 2, 2019

REFERENCES

Boles, B.R., Thoendel, M., Roth, A.J., and Horswill, A.R. (2010). Identification of genes involved in polysaccharide-independent *Staphylococcus aureus* biofilm formation. PLoS One *5*, e10146.

Bussey, R.O., 3rd, Kaur, A., Todd, D.A., Egan, J.M., El-Elimat, T., Graf, T.N., Raja, H.A., Oberlies, N.H., and Cech, N.B. (2015). Comparison of the chemistry and diversity of endophytes isolated from wild-harvested and greenhouse-cultivated yerba mansa (*Anemopsis californica*). Phytochem. Lett. *11*, 202–208.

Carroll, R.K., Weiss, A., Broach, W.H., Wiemels, R.E., Mogen, A.B., Rice, K.C., and Shaw, L.N. (2016). Genome-wide annotation, identification, and global transcriptomic analysis of regulatory or small RNA gene expression in Staphylococcus aureus. MBio *7*, e01990–e15.

CDC (2013). Antibiotic resistance threats in the United States, 2013. (Report from the Centers for Disease Control). https://www.cdc.gov/drugresistance/pdf/ar-threats-2013-508.pdf.

Cech, N.B., and Horswill, A.R. (2013). Small-molecule quorum quenchers to prevent Staphylococcus aureus infection. Future Microbiol. *8*, 1511–1514.

Cegelski, L., Marshall, G.R., Eldridge, G.R., and Hultgren, S.J. (2008). The biology and future prospects of antivirulence therapies. Nat. Rev. Microbiol. *6*, 17–27.

Chambers, H.F., and Deleo, F.R. (2009). Waves of resistance: Staphylococcus aureus in the antibiotic era. Nat. Rev. Microbiol. *7*, 629–641.

Cheung, G.Y., Wang, R., Khan, B.A., Sturdevant, D.E., and Otto, M. (2011). Role of the accessory gene regulator agr in community-associated methicillin-resistant Staphylococcus aureus pathogenesis. Infect. Immun. *79*, 1927–1935.

Crosby, H.A., Schlievert, P.M., Merriman, J.A., King, J.M., Salgado-Pabón, W., and Horswill, A.R. (2016). The Staphylococcus aureus global regulator MgrA modulates clumping and virulence by controlling surface protein expression. PLoS Pathog. *12*, e1005604.

Daly, S.M., Elmore, B.O., Kavanaugh, J.S., Triplett, K.D., Figueroa, M., Raja, H.A., El-Elimat, T., Crosby, H.A., Femling, J.K., Cech, N.B., et al. (2015). ω-Hydroxyemodin limits staphylococcus aureus quorum sensing-mediated pathogenesis and inflammation. Antimicrob. Agents Chemother. *59*, 2223–2235.

DeLeo, F.R., and Chambers, H.F. (2009). Reemergence of antibiotic-resistant Staphylococcus aureus in the genomics era. J. Clin. Invest. *119*, 2464–2474.

DeLeo, F.R., Otto, M., Kreiswirth, B.N., and Chambers, H.F. (2010). Community-associated meticillin-resistant Staphylococcus aureus. Lancet *375*, 1557–1568.

El-Elimat, T., Figueroa, M., Ehrmann, B.M., Cech, N.B., Pearce, C.J., and Oberlies, N.H. (2013). High-resolution MS, MS/MS, and UV database of fungal secondary metabolites as a dereplication protocol for bioactive natural products. J. Nat. Prod. *76*, 1709–1716.

Figueroa, M., Jarmusch, A.K., Raja, H.A., El-Elimat, T., Kavanaugh, J.S., Horswill, A.R., Cooks, R.G., Cech, N.B., and Oberlies, N.H. (2014). Polyhydroxyanthraquinones as quorum sensing inhibitors from the guttates of Penicillium restrictum and their analysis by desorption electrospray ionization mass spectrometry. J. Nat. Prod. *77*, 1351–1358.

Geisinger, E., Muir, T.W., and Novick, R.P. (2009). agr receptor mutants reveal distinct modes of inhibition by staphylococcal autoinducing peptides. Proc. Natl. Acad. Sci. USA *106*, 1216–1221.

Gordon, C.P., Williams, P., and Chan, W.C. (2013). Attenuating Staphylococcus aureus virulence gene regulation: a medicinal chemistry perspective. J. Med. Chem. *56*, 1389–1404.

Gordon, C.P., Olson, S.D., Lister, J.L., Kavanaugh, J.S., and Horswill, A.R. (2016). Truncated autoinducing peptides as antagonists of Staphylococcus lugdunensis quorum sensing. J. Med. Chem. *59*, 8879–8888.

Hall, P.R., Elmore, B.O., Spang, C.H., Alexander, S.M., Manifold-Wheeler, B.C., Castleman, M.J., Daly, S.M., Peterson, M.M., Sully, E.K., Femling, J.K., et al. (2013). Nox2 modification of LDL is essential for optimal apolipoprotein B-mediated control of agr type III Staphylococcus aureus quorum-sensing. PLoS Pathog. *9*, e1003166.

Kavanaugh, J.S., and Horswill, A.R. (2016). Impact of environmental cues on Staphylococcal quorum sensing and biofilm development. J. Biol. Chem. *291*, 12556–12564.

Kiedrowski, M.R., Kavanaugh, J.S., Malone, C.L., Mootz, J.M., Voyich, J.M., Smeltzer, M.S., Bayles, K.W., and Horswill, A.R. (2011). Nuclease modulates biofilm formation in community-associated methicillin-resistant Staphylococcus aureus. PLoS One *6*, e26714.

Kirchdoerfer, R.N., Garner, A.L., Flack, C.E., Mee, J.M., Horswill, A.R., Janda, K.D., Kaufmann, G.F., and Wilson, I.A. (2011). Structural basis for ligand recognition and discrimination of a quorum-quenching antibody. J. Biol. Chem. *286*, 17351–17358.

Laxminarayan, R., Duse, A., Wattal, C., Zaidi, A.K., Wertheim, H.F., Sumpradit, N., Vlieghe, E., Hara, G.L., Gould, I.M., Goossens, H., et al. (2013). Antibiotic resistance—the need for global solutions. Lancet Infect. Dis. *13*, 1057–1098.

Limbago, B., Fosheim, G.E., Schoonover, V., Crane, C.E., Nadle, J., Petit, S., Heltzel, D., Ray, S.M., Harrison, L.H., Lynfield, R., et al. (2009). Characterization of methicillin-resistant Staphylococcus aureus isolates collected in 2005 and 2006 from patients with invasive disease: a population-based analysis. J. Clin. Microbiol. *47*, 1344–1351.

Lowy, F.D. (1998). Staphylococcus aureus infections. N. Engl. J. Med. *339*, 520–532.

Mayville, P., Ji, G., Beavis, R., Yang, H., Goger, M., Novick, R.P., and Muir, T.W. (1999). Structure-activity analysis of synthetic autoinducing thiolactone peptides from Staphylococcus aureus responsible for virulence. Proc. Natl. Acad. Sci. USA *96*, 1218–1223.

Medina, E., and Pieper, D.H. (2016). Tackling threats and future problems of multidrug-resistant bacteria. Curr. Top. Microbiol. Immunol. *398*, 3–33.

Miller, L.S., and Cho, J.S. (2011). Immunity against Staphylococcus aureus cutaneous infections. Nat. Rev. Immunol. *11*, 505–518.

Moran, G.J., Krishnadasan, A., Gorwitz, R.J., Fosheim, G.E., McDougal, L.K., Carey, R.B., Talan, D.A., et al. (2006). Methicillin-resistant S. aureus infections among patients in the emergency department. N. Engl. J. Med. *355*, 666–674.

Muhs, A., Lyles, J.T., Parlet, C.P., Nelson, K., Kavanaugh, J.S., Horswill, A.R., and Quave, C.L. (2017). Virulence inhibitors from Brazilian peppertree block quorum sensing and abate dermonecrosis in skin infection models. Sci. Rep. *7*, 42275.

NIAID (2014). NIAID's Antibacterial Resistance Program: Current status and future directions. Report of the National Institute of Allergy and Infectious Diseases. https://www.niaid.nih.gov/sites/default/files/arstrategicplan2014.pdf.

Nielsen, A., Månsson, M., Bojer, M.S., Gram, L., Larsen, T.O., Novick, R.P., Frees, D., Frøkiær, H., and Ingmer, H. (2014). Solonamide B inhibits quorum sensing and reduces Staphylococcus aureus mediated killing of human neutrophils. PLoS One *9*, e84992.

Novick, R.P., and Geisinger, E. (2008). Quorum sensing in staphylococci. Annu. Rev. Genet. *42*, 541–564.

O'Neill, J. (2016). Tackling Drug-Resistant Infections Globally. (Wellcome Trust).

Otto, M. (2010). Basis of virulence in community-associated methicillin-resistant Staphylococcus aureus. Annu. Rev. Microbiol. *64*, 143–162.

Paharik, A.E., Parlet, C.P., Chung, N., Todd, D.A., Rodriguez, E.I., Van Dyke, M.J., Cech, N.B., and Horswill, A.R. (2017). Coagulase-negative Staphylococcal strain prevents Staphylococcus aureus colonization and skin infection by blocking quorum sensing. Cell Host Microbe *22*, 746–756.e5.

Pang, Y.Y., Schwartz, J., Thoendel, M., Ackermann, L.W., Horswill, A.R., and Nauseef, W.M. (2010). agr-dependent interactions of Staphylococcus aureus USA300 with human polymorphonuclear neutrophils. J. Innate Immun. *2*, 546–559.

Quave, C.L., and Horswill, A.R. (2014). Flipping the switch: tools for detecting small molecule inhibitors of staphylococcal virulence. Front Microbiol. *5*, 706.

Quave, C.L., Lyles, J.T., Kavanaugh, J.S., Nelson, K., Parlet, C.P., Crosby, H.A., Heilmann, K.P., and Horswill, A.R. (2015). Castanea sativa (European Chestnut) Leaf Extracts Rich in Ursene and Oleanene Derivatives Block Staphylococcus aureus Virulence and Pathogenesis without Detectable Resistance. PLoS One *10*, e0136486.

Queck, S.Y., Jameson-Lee, M., Villaruz, A.E., Bach, T.H., Khan, B.A., Sturdevant, D.E., Ricklefs, S.M., Li, M., and Otto, M. (2008). RNAIII-independent target gene control by the agr quorum-sensing system: insight into the evolution of virulence regulation in Staphylococcus aureus. Mol. Cell *32*, 150–158.

Raja, H.A., Miller, A.N., Pearce, C.J., and Oberlies, N.H. (2017). Fungal identification using molecular tools: A primer for the natural products research community. J. Nat. Prod. *80*, 756–770.

Rasko, D.A., and Sperandio, V. (2010). Anti-virulence strategies to combat bacteria-mediated disease. Nat. Rev. Drug Discov. *9*, 117–128.

Spaan, A.N., Surewaard, B.G., Nijland, R., and van Strijp, J.A. (2013). Neutrophils versus Staphylococcus aureus: a biological tug of war. Annu. Rev. Microbiol. *67*, 629–650.

Spellberg, B., Bartlett, J., Wunderink, R., and Gilbert, D.N. (2015). Novel approaches are needed to develop tomorrow's antibacterial therapies. Am. J. Respir. Crit. Care Med. *191*, 135–140.

Spellberg, B., Srinivasan, A., and Chambers, H.F. (2016). New societal approaches to empowering antibiotic stewardship. JAMA *315*, 1229–1230.

Sully, E.K., Malachowa, N., Elmore, B.O., Alexander, S.M., Femling, J.K., Gray, B.M., DeLeo, F.R., Otto, M., Cheung, A.L., Edwards, B.S., et al. (2014). Selective chemical inhibition of agr quorum sensing in Staphylococcus aureus promotes host defense with minimal impact on resistance. PLoS Pathog. *10*, e1004174.

Thoendel, M., Kavanaugh, J.S., Flack, C.E., and Horswill, A.R. (2011). Peptide signaling in the staphylococci. Chem. Rev. *111*, 117–151.

Todd, D.A., Parlet, C.P., Crosby, H.A., Malone, C.L., Heilmann, K.P., Horswill, A.R., and Cech, N.B. (2017). Signal biosynthesis inhibition with ambuic acid as a strategy to target antibiotic-resistant infections. Antimicrob Agents Chemother *61*, e00263-00217.

Tong, S.Y., Davis, J.S., Eichenberger, E., Holland, T.L., and Fowler, V.G.J., Jr. (2015). Staphylococcus aureus infections: epidemiology, pathophysiology, clinical manifestations, and management. Clin. Microbiol. Rev. *28*, 603–661.

Wright, J.S., 3rd, Jin, R., and Novick, R.P. (2005). Transient interference with staphylococcal quorum sensing blocks abscess formation. Proc. Natl. Acad. Sci. USA *102*, 1691–1696.

STAR★METHODS

KEY RESOURCES TABLE

REAGENT or RESOURCE	SOURCE	IDENTIFIER
Antibodies		
anti-mouse Ly6G (1A8)	Biolegend	Cat# 127614
anti-mouse Ly6C (HK1.4)	Biolegend	Cat# 128016
anti-mouse CD45 (30-F11)	Biolegend	Cat# 103134
anti-mouse CD31 (390)	Biolegend	Cat# 102412
anti-mouse/human CD11b (M1/70)	Biolegend	Cat# 101226
rat anti-mouse CD16/32 FcγRIII/II (2.4G2)	Dr. Thomas Waldschmidt, Univ. of Iowa	N/A
Bacterial and Virus Strains		
Chaetosphaeriaceae sp. [Sordariomycetes, Ascomycota]	Mycosynthetix	MSX53644
Fusarium sp.	This work	G134
Fusarium sp.	This work	G137
S. aureus Restriction deficient cloning host	Lab collection	RN4220
S. aureus MN EV, agr type IV	Lab collection	AH407
S. aureus 502a + pDB59 cm^R, YFP reporter, agr type II	Lab collection	AH430
S. aureus MW2, agr type III	Lab collection	AH843
S. aureus USA300 agr type I	Boles et al., 2010	AH845
S. aureus USA300 CA-MRSA Erm^S (LAC*)	Boles et al., 2010	AH1263
LAC* Δagr::tet	Kiedrowski et al., 2011	AH1292
AH845 + pDB59 cm^R, YFP reporter, agr type I	Kirchdoerfer et al., 2011	AH1677
MW2 + pDB59 cm^R, YFP reporter, agr type III	Kirchdoerfer et al., 2011	AH1747
MN EV + pDB59 cm^R; YFP reporter, agr type IV	Kirchdoerfer et al., 2011	AH1872
LAC* agrP3::luxABCDE	Figueroa et al., 2014	AH2759
LAC* Δ*agr*::tet + pCM29 cmR (GFP)	Paharik et al., 2017	AH2768
LAC* Δ*agr*::tet, φ11::LL29 *sarA*P1-*agrBD*	Todd et al., 2017	AH2989
RN4220 Δ*agr*::*ermB agr*P3::*luxABCDE* + pEPSA5-*agrA*	Sully et al., 2014	AH3048
JE2 *agrC*::ΦNΣ, φ11::LL29 + pRMC2-*agrBDCA*	Daly et al., 2015	AH3469
JE2 *agrC*::ΦNΣ, φ11::LL29 + pRMC2-*agrBDCA* (*agrC* R238H)	Daly et al., 2015	AH3470
LAC* + pCM29 cm^R (GFP)	Pang et al., 2010	AH3669
S. aureus USA100 MRSA blood isolate IA116	Daniel Diekema	AH3684
LAC* Lux	Todd et al., 2017	AH3700
LAC* Δ*agr*::tet Lux	Paharik et al., 2017	AH3774
USA100 IA116 *agr*P3::*luxABCDE*	This work	AH4390
Biological Samples		
Rabbit defibrinated blood 250 mL	HemoStat Laboratories	Cat# DRB250
Chemicals, Peptides, and Recombinant Proteins		
Trypsin	VWR Life Sciences	Cat# 90002-07-7
Collagenase Type II	Gibo	Cat# 9001-12-1
Propidium iodide	Biolegend	Cat# 421301
Annexin V	Biolegend	Cat# 640919
Chloramphenicol	Sigma	Cat# C0378
Ambuic acid	Apidogen Life Sciences	Cat# AG-CN2-0129-M001
S. aureus AIP-II	Anaspec	Peptide# 61088
Apicidin	Sigma	Cat# A8851

(*Continued on next page*)

Continued

REAGENT or RESOURCE	SOURCE	IDENTIFIER
RNAprotect	QIAGEN	Cat# 76526
Lysostaphin	Sigma	Cat# L7386
Formic Acid (Optima Grade)	Fisher Scientific	Cat# A117-50
Acetonitrile (Optima Grade)	Fisher Scientific	Cat# A955-4
Acetonitrile (HPLC Grade)	Fisher Scientific	Cat# A998SK-4
Water (Optima Grade)	Fisher Scientific	Cat# W6-4
Stemsol (DMSO)	Protide Pharmaceuticals	Cat# PP1350
Critical Commercial Assays		
Mouse magnetic Luminex Assay	R&D Systems	Custom
RNeasy Mini kit	QIAGEN	Cat# 74104
Turbo DNA-free kit	Fisher Scientific	Cat# AM1907
Ribo-Zero rRNA Removal Kit (Gram-Positive Bacteria)	Illumina	Cat# MRZGP126
TruSeq Stranded mRNA Library Prep Kit	Illumina	Cat# RS-122-2103
Deposited Data		
RNaseq data	This work	GenBank: SRP182661
Chaetosphaeriaceae sp. ITS spacer and 28S rRNA	This work	GenBank: MF374619
Fusarium sp. G134 ITS spacer	This work	GenBank: KM816766
Fusarium sp. G137 ITS spacer	This work	GenBank: KM816768
Experimental Models: Organisms/Strains		
C57BL/6N mice	Charles River Laboratories	Strain code 027
BALB/c mice	Charles River Laboratories	Strain code 028
Oligonucleotides		
CTTGGTCATTTAGAGGAAGTAA	IDT	ITS1F
TCCTCCGCTTATTGATATGC	IDT	ITS4
Software and Algorithms		
Living Image Software	Xenogen	Version 4.4
Flow Jo	TreeStar	Version 10.4
FACSDiva	BD	Version 8
CellQuest	BD	Version 5.1
ImageJ	NIH	N/A
Galaxie Chromatography Workstation	Varian	Version 1.9.3.2
SeqMan NGen	DNASTAR	Version 14
ArrayStar	DNASTAR	Version 14
PRISM	GraphPad	Version 7.0a
Other		
TECAN plate reader	TECAN LifeSciences	Infinite M200
Stuart SI505 Microplate Shaking Incubator	Cole-Parmer	Item # EW-79520-08
Xenogen *in vivo* imaging system (IVIS)	Caliper Life Sciences	IVIS200
CombiFlash RF system	Teledyne-Isco	Unit ID: 625230006
Q Exactive Plus orbitrap mass spectrometer	Thermo Fisher	N/A
Acquity UPLC	Waters	Product No: Photodiode Array eλ Detector – 186015033
Acquity UPLC	Waters	Column Manager – 800000247
Acquity UPLC	Waters	Sample Manager – 186015006
Acquity UPLC	Waters	Binary Solvent Manager – 186015001
Acquity BEH C18 UPLC column	Waters	186002350
Prostar HPLC	Varian	N/A
Gemini-NX C_{18} (analytical)	Phenomenex	00G-4435-E0

(*Continued on next page*)

Continued

REAGENT or RESOURCE	SOURCE	IDENTIFIER
Gemini-NX C_{18} (preparative)	Phenomenex	00G-4435-P0-AX
130 g Redisep RF C18 column	Teledyne-Isco	Cat# 69-2203-337
LTQ Orbitrap XL mass spectrometer	Thermo Fisher	N/A
ECA-500 NMR Spectrometer	JEOL	N/A
Luminex 200	Luminex	N/A
FACS LSR II	BD	N/A

CONTACT FOR REAGENT AND RESOURCE SHARING

Further information and request for resources should be forwarded to and will be fulfilled by the Lead Contact, Dr. Alexander R. Horswill (alexander.horswill@ucdenver.edu).

EXPERIMENTAL MODEL AND SUBJECT DETAILS

Bacterial strains and plasmids

For all experiments, *S. aureus* cultures were grown in a tryptic soy broth (TSB) at 37°C with shaking at 200 rpm. Chloramphenicol (Cam) was added to the media as needed at 10 μg/mL. Bacterial strains used are listed specifically in each method section and in the Key Resource Table.

Mice

C57BL/6N or BALB/c mice (equal male and female numbers) were purchased from the Charles River and housed in specific pathogen free facilities at the University of Iowa. Prior to their inclusion in the study, mice were allowed to acclimate to the ABSL-2 animal housing facility at the University of Iowa for at least seven days. For *in vivo* studies, 8 to 20-week old age-matched, sex-matched mice were randomly assigned to treatment groups and at experimental end points, mice were humanely euthanized using carbon dioxide inhalation. The animal studies were reviewed and protocol approved by the University of Iowa Institutional Animal Care and Use Committee. The University of Iowa is AAALAC accredited, and the centralized facilities meet and adhere to the standards in the "Guide and Care of Laboratory Animals."

Plant material

Plant material of yerba mansa [*Anemopsis californica* (Nutt.) Hook. & Arn. (Saururaceae)] was collected with permission by Amy Brown of Apache Creek Ranch in Santa Fe, NM (35°35′ 56.40″N, 105°50′ 27.22″W). A voucher specimen (NCU602027) was deposited in the University of North Carolina Herbarium. The specimen was authenticated by Amy Brown.

Fungal strains

Fungal strain MSX53644 from Mycosynthetix library was stored, fermented, and extracted via well-established methods. Based on GenBank BLAST search and molecular phylogenetic analysis using the internal transcribed spacers (ITS1-5.8S-ITS2) region and the D1-D2 variable portion of the 28S rRNA large subunit gene of the nuclear RNA operon, as detailed previously (Raja et al., 2017), MSX53644 was identified as Chaetosphaeriaceae sp. [Sordariomycetes, Ascomycota] (Figure S2D). The sequence data were deposited in GenBank under accession numbers: MF374619, MF374620, MF374621, MF374622.

The endophytic fungal strains G134 and G137 were isolated from surface sterilized fresh roots of yerba mansa [*Anemopsis californica* (Nutt.) Hook. & Arn. (Saururaceae)] using methods reported in detail previously (Bussey et al., 2015). Strains G134 and G137 were found to be two isolates for the same strain and were identified as a *Fusarium* sp. by sequencing the internal transcribed spacer region of the ribosomal RNA gene (ITS) using molecular methods (Raja et al., 2017). The ITS sequences for G134 and G137 were deposited in GenBank (accession number KM816766 for G134 and KM816768 for G137).

METHOD DETAILS

Quenching assays with reporter strains:

Apicidin was tested for quorum quenching activity against all four *agr* types using P3-YFP reporter strains AH1677 (type I), AH430 (type II), AH1747 (type III), and AH1872 (type IV) (Hall et al., 2013; Kirchdoerfer et al., 2011). Overnight cultures of reporter strains that were grown in TSB supplemented with Cam were inoculated at a dilution of 1:250 into fresh TSB containing Cam. 100 μL aliquots were added to 96-well microtiter plates containing 100 μL aliquots of TSB containing Cam and 2-fold serial dilutions of apicidin. Readings were recorded at 30 min increments using a Tecan Systems Infinite M200 plate reader.

Hemolytic activity

A rabbit red blood cell (RBC) hemolysis assay based on previously described methods was used (Daly et al., 2015; Pang et al., 2010). Overnight cultures of *agr* strain types I, II, III, and IV were inoculated 1:500 into 5 mL of TSB (in 17x150 mm culture tubes) containing apicidin at concentrations of 100, 50, 25, 12.5, and 6.25 μg/mL. For assessing the impact on constitutive AgrC, strains AH3469 and AH3470 were used in parallel with apicidin treatment as previously described (Daly et al., 2015). All cultures were incubated at 37°C with shaking (250 rpm), and growth was monitored by periodically transferring 100 μL of culture to a 96-well microtiter plate and reading OD_{600} in a Tecan Systems Infinite M200 plate reader. Following incubation, 600 μL of each culture was filter sterilized using cellulose acetate SpinX 0.22 μm filters. To quantify hemolytic activity, the filter sterilized culture supernatants from apicidin treated cultures were diluted, and 50 μL aliquots were dispensed in quadruplicate into 96-well microtiter plates. Rabbit erythrocytes, were added to the microtiter plates at 50 μL per well. The erythrocytes and culture supernatants were mixed and incubated statically at room temperature for 2 hr. Hemolysis was detected by the loss of turbidity as measured at OD_{630} using a Tecan Infinite M200 plate reader.

Mass Spectrometric Measurements of AIP

Experiments to evaluate the impact of apicidin on signal biosynthesis by MRSA were conducted as described previously (Todd et al., 2017). Briefly, 250 μL cultures of strains AH2989 (AIP constitutively producing strain (Todd et al., 2017)) and AH1263 (wild-type, USA300 LAC (Boles et al., 2010)) were treated with 5 μL of 5 mM apicidin in DMSO, for a final concentration of 100 μM in the culture media. The known signal biosynthesis inhibitor ambuic acid (also at 100 μM) served as a positive control, and vehicle (2% DMSO in TSB) served as negative control. AIP I levels produced by both strains after 18 hr were measured directly from spent media using ultraperformance liquid chromatography (Waters Acquity UPLC) coupled to high resolution mass spectrometry (Q-Exactive Orbitrap, Thermo).

Fermentation, extraction and isolation

For chemistry studies, a 2.8-L Fernbach flask (Corning, Inc., Corning, NY, USA) containing 150 g rice and 300 mL H_2O was inoculated with as seed culture this strain that was grown in YESD medium. After incubation for 14 days at r.t., the solid culture was extracted by addition of a 500 mL mixture of 1:1 MeOH/$CHCl_3$. Using a spatula, the culture was chopped into small pieces and left to shake at 125 rpm at r.t., followed by filtration. The solid residues were then washed with 100 mL of 1:1 MeOH/$CHCl_3$. To the combined filtrates, 900 mL $CHCl_3$ and 1500 mL H_2O were added so that the final ratio of $CHCl_3$/MeOH/H_2O was 4:1:5 and left to stir for 30 min. The mixture was then transferred into as a separatory funnel and the organic bottom layer was drawn off and evaporated to dryness. The dried organic phase was then re-constituted in 100 mL of 1:1 MeOH/CH_3CN and 100 mL of hexanes and transferred into a separatory funnel. The MeOH/CH_3CN layer was drawn off and evaporated to dryness under vacuum. The defatted crude material (1.2 g) was dissolved in a mixture of $CHCl_3$/MeOH, adsorbed onto Celite 545, and fractionated via normal phase flash chromatography using a gradient solvent system of hexane/$CHCl_3$/MeOH at a 40 mL/min flow rate and 53.3 column volumes over 63.9 min to afford five fractions. Fraction 4 (300 mg) was subjected to preparative reversed-phase HPLC over a Phenomenex Gemini-NX C_{18} preparative column using a gradient system of 40:60 to 70:30 over 30 min of CH_3CN/H_2O (acidified with 0.1% formic acid) at a flow rate of 21.24 mL/min (Figure 1F) to yield compounds **1** (4.1 mg) and **2** (3.0 mg) which eluted at 18.0 and 19.5 min, respectively. The HRMS (Figure S1A) and ^1H and ^{13}C NMR data (Figure S1B) for compounds **1** and **2** were in agreement with the literature.

Fermentation, extraction and isolation of compounds from strains G134 and G137

Strains G134 and G137 were fermented and extracted using techniques akin to those described for strain MSX53644 above. The extracts from G134 and G137 were combined, as the LC-MS analysis of the extracts showed similar chemical profiles, the two cultures showed similar morphological characteristics, and decisively, the two isolates showed similar sequences of the internal transcribed spacer region of the ribosomal RNA gene (ITS). The combined defatted extracts of G134 and G137 (125 mg) were then fractionated using normal phase flash chromatography using a gradient solvent system of hexane/$CHCl_3$/MeOH at a 18 mL/min flow rate and 68.1 column volumes over 18.2 min to afford five fractions. Fraction 5 (35 mg) was found to contain apicidin as evidenced by LC-MS analysis and hence was subjected to preparative reversed-phase HPLC purification over a Phenomenex Gemini-NX C_{18} preparative column using a gradient system of 40:60 to 70:30 over 30 min of CH_3CN/H_2O (acidified with 0.1% formic acid) at a flow rate of 21.24 mL/min (Figure 1F) to yield compounds **2** (8.9 mg), **3** (1.7 mg), and **4** (1.5 mg), which eluted at 19.5, 15.5, and 17.5 min, respectively. The HRMS (Figure S1A) and ^1H and ^{13}C NMR data (Figure S1B) for compounds **2**, **3** and **4** were in agreement with the literature.

NMR methods

NMR data were collected using a JEOL ECA-500 NMR spectrometer operating at 500 MHz for ^1H and 125 MHz for ^{13}C (JEOL Ltd., Tokyo, Japan). Residual solvent signals were utilized for referencing. High resolution mass spectra (HRMS) were obtained using a Thermo LTQ Orbitrap XL mass spectrometer equipped with an electrospray ionization source (Thermo Fisher Scientific, San Jose, CA, USA). Phenomenex Gemini-NX C_{18} analytical (5 μm; 250 × 4.6 mm) and preparative (5 μm; 250 × 21.2 mm) columns (Phenomenex, Torrance, CA, USA) were used on a Varian Prostar HPLC system equipped with ProStar 210 pumps and a Prostar 335 photodiode array detector (PDA), with data collected and analyzed using Galaxie Chromatography Workstation software (version

1.9.3.2, Varian Inc.). Flash chromatography was conducted on a Teledyne ISCO CombiFlash Rf using Silica Gold columns and monitored by UV and evaporative light-scattering detectors (both from Teledyne Isco, Lincoln, NE, USA).

S. aureus skin infections

At D0, age, strain and sex matched C57BL/6 or BALB/c mice were anesthetized with isoflurane, abdominal skin was carefully shaved and exposed skin was cleansed by wiping with an alcohol prep pad. For inoculum preparation, a USA300 MRSA LAC strain (AH1263) (Boles et al., 2010), and strains engineered for constitutive bioluminescence via *lux* operon insertion (AH3700) or its *agr* null counterpart (AH2989), or the LAC WT engineered to constitutively express green fluorescent protein (AH3669) or its *agr* null counterpart (AH2768), were grown to mid-log-phase, pelleted and resuspended in DPBS to achieve 50 μL inoculum mixtures that contained either 2 x10^7 CFUs ± 5 μg apicidin (diluted in neat DMSO). Apicidin or DMSO containing inoculums were injected intradermally into abdominal skin. Baseline body weights of mice were measured before infection and every day thereafter for a period of 7-14 days. For determination of lesion size, digital photos of skin lesions were taken daily and analyzed via ImageJ software. For the USA100 experiments, strain AH3684 (IA116, kindly provided by Dr. Daniel Diekema) was used. The plasmid for *agr*-P3 lux was transformed into this strain for monitoring *agr* kinetics during infection (new strain AH4390).

Measurement of quorum quenching *in vivo*

Inoculum preparation for assessing quorum quenching *in vivo*. An MRSA LAC reporter strain engineered to couple *agr* activation with bioluminescence, called *agr*-P3 lux (AH2759) (Figueroa et al., 2014), was grown in TSB medium containing chloramphenicol overnight at 37°C in a shaking incubator set to 200 rpm. Overnight cultures were diluted 1:100 TSB with chloramphenicol and subcultured to an optical density of 0.1 at 600nm (≈1 hr). Bacterial cells were then pelleted and resuspended in sterile saline. 50 μL inoculum suspensions containing 1x10^7 CFUs and 5 μg of apicidin diluted in DMSO or DMSO alone were injected intradermally into abdominal skin using 0.3 mL/31 gauge insulin syringe (as a technical control several mice were injected in the same manner with 50 μL of sterile saline only. For all infections, challenge dose was confirmed by plating serial dilutions of inoculum on TSA and counting ensuing colonies after overnight culture. Beginning immediately after infection, mice were imaged under isoflurane inhalation anesthesia (2%). Photons emitted from luminescent bacteria were collected during a 2 min exposure using the Xenogen IVIS Imaging System and living image software (Xenogen, Alameda, CA). Bioluminescent image data are presented on a pseudocolor scale (blue representing least intense and red representing the most intense signal) overlaid onto a gray-scale photographic image. Using the image analysis tools in living image software, circular analysis windows (of uniform area) were overlaid onto abdominal regions of interest, and the corresponding bioluminescence values (total flux) were measured and plotted versus time after infection.

Evaluation of skin and blood immune cells

For skin: abdominal skin ulcerations were excised and incubated in trypsin (0.6% in PBS) for 75 min at 37°C; then cut into small pieces and incubated in Collagenase type II (0.5 mg/mL RPMI) for 90 min at 37°C. Skin cell suspensions were generated by serial passage of skin fragments through 18 and 20 gauge syringes. LN cell suspensions were generated mincing inguinal LNs with a razor blade before serial passage of LN fragments through 18 and 20 gauge syringes. For whole blood: blood was collected, washed and re-suspended in Tris-buffered ammonium chloride to lyse red blood cells. All tissue preps were passed through a 70 μm filter before staining.

Whole blood killing assays

For killing assays: PB was collected in sodium heparin tubes, transferred into round bottomed 96 well plates (Corning, NY). LAC cultures were grown in the presence of apicidin (100 μM) or DMSO for 4 hr at 37°C with shaking (250 rpm). After culture, cells were washed in saline and resuspended to a concentration of ≈1x10^5 CFUs/μL. Cells exposed to Apicidin or control were then mixed with heparinized PB in at a concentration of 1x10^6 CFUs/150 μL PB, the infected blood was incubated at 37°C in a 37°C with shaking (250 rpm). After 1 h, serial dilutions in saline were performed to determine the endpoint numbers of CFU, which were compared to the initial bacterial load to determine the viable percentage of the initial inoculum.

RNA Seq

RNaseq was essentially performed as previously described (Crosby et al., 2016). Briefly, cultures of LAC and LACΔ*agr* were grown in TSB with DMSO alone or 100 μM apicidin (diluted in neat DMSO) in triplicate in a 48-well plate. Cultures were grown to optical density of 4 at 600 nm, and cells were harvested and treated with RNAProtect Bacteria Reagent (QIAGEN). Cells were lysed using lysostaphin and RNA purified using the RNeasy mini kit (QIAGEN). The samples were treated with DNA-free (Ambion) and sample quality was affirmed via Bioanalyzer (Agilent). Ribosomal RNA was depleted using Ribo-Zero rRNA Removal Kit for gram positive bacteria (Illumina). cDNA libraries were generated at the University of Iowa Genomics Division using the TruSeq Stranded mRNA Library Prep kit (Illumina). Sample were barcoded, pooled and sequenced in 125x125 paired-end reads on an Illumina HiSeq 2000 sequencer. The resulting reads were aligned to an updated *S. aureus* USA300 genome file containing annotations for small RNAs (Carroll et al., 2016) using SeqMan NGen (DNASTAR) and reads were quantified using ArrayStar (DNASTAR). Genes were considered differentially expressed if they showed a ≥ 4-fold change in expression with 95% confidence as evaluated by Student's t test with a false discovery rate (FDR) correction applied for multiple t tests.

Flow cytometry

For staining of skin, LN and whole blood preparations, the following antibodies: Anti-Ly6G (1A8), Anti-Ly6C (HK1.4), -CD11b (M1/70), CD45 (30-F11) were purchased from BioLegend. To block nonspecific binding, cells were incubated with rat anti-mouse CD16/32 FcγRIII/II (2.4G2) and vortexed prior to surface staining. In all experiments, cells were collected on a LSR II using Diva software, and analyzed using FlowJo software. Dead cells were excluded by low forward-scatter and side-light scatter. Spectral overlaps between fluorochrome channels were corrected by automated compensation on singly stained, positive controls for each fluorochrome. In general, 50,000 cells were collected/tube. Flow cytometric analyses of bacterial cultures were conducted by incubating MRSA subcultures in 100 μM apicidin, for the 4 or 7 hr in a Stuart incubator set to 37°C, shaking at 1000 RPM. After, washing and resuspending cultures in DPBS, samples were collected on a FACS LSR II using Diva software.

Cytokine Measurements from Tissue Homogenates

Biopsy punches (4 mm), obtained from the center of skin ulcerations 1 day after infection, were homogenized with in sterile RPMI with proteinase inhibitor cocktail. The supernatants from these preparations were incubated with a multiplex bead array for IL-1β, G-CSF, KC (CXCL1), and CXCL2. Data were collected on a Luminex 200 (Luminex, Austin, TX, USA) and analyzed with Bio-plex manager software 6.0.

QUANTIFICATION AND STATISTICAL ANALYSIS

Statistics

For each experiment, the total number of replicates (n) and the statistical tests performed can be found in the figure legends. With the exception of flow cytometry and bioluminescent imaging data, all analyses were performed using GraphPad PRISM software version 7 (GraphPad Software, Inc. La Jolla, CA). Throughout this work, significance was defined as $p < 0.05$. The *P value*s for comparisons between experimental groups were calculated by use of an unpaired Student's t test. Error is presented as standard error of the mean (SEM) unless otherwise noted.

For the RNaseq experiments, expression data was analyzed with ArrayStar (DNASTAR) and genes were considered differentially expressed if they showed a $\geq$ 4-fold change with 95% confidence as evaluated by Student's t test with a false discovery rate (FDR) correction applied for multiple t tests.

DATA AND SOFTWARE AVAILABILITY

The RNaseq results with LAC (+/− apicidin treatment) and the Δ*agr* mutant were uploaded to the NCBI GEO database. Accession information: https://www.ncbi.nlm.nih.gov/sra?term=SRP182661.